Full Paper

www.molinf.com

molecular informatics

DOI: 10.1002/minf.202000115

In silico Drug Repurposing for COVID-19: Targeting SARS-CoV-2 Proteins through Docking and Consensus Ranking

Claudio N. Cavasotto*[a, b, c] and Juan I. Di Filippo[a]

Abstract: In December 2019, an infectious disease caused by the coronavirus SARS-CoV-2 appeared in Wuhan, China. This disease (COVID-19) spread rapidly worldwide, and on March 2020 was declared a pandemic by the World Health Organization (WHO). Today, over 21 million people have been infected, with more than 750.000 casualties. Today, no vaccine or antiviral drug is available. While the development of a vaccine might take at least a year, and for a novel drug, even longer; finding a new use to an old drug (drug repurposing) could be the most effective strategy. We present a docking-based screening using a quantum mechanical scoring of a library built from approved drugs and compounds undergoing clinical trials, against three SARS-CoV-2 target proteins: the spike or S-protein, and two proteases, the main protease and the papain-like protease. The S-protein binds directly to the Angiotensin Converting Enzyme 2 receptor of the human host cell surface, while the two proteases process viral polyproteins. Following the analysis of our structure-based compound screening, we propose several structurally diverse compounds (either FDA-approved or in clinical trials) that could display antiviral activity against SARS-CoV-2. Clearly, these compounds should be further evaluated in experimental assays and clinical trials to confirm their actual activity against the disease. We hope that these findings may contribute to the rational drug design against COVID-19.

Keywords: Molecular Docking · Consensus Scoring · Quantum Mechanical Scoring · COVID-19, SARS-CoV-2 · Drug Repurposing

1 Introduction

Coronaviruses (CoVs) usually are the cause of mild to serious respiratory tract infections. In the past decades, two highly pathogenic CoVs, the severe acute respiratory syndrome coronavirus (SARS-CoV) and the Middle East respiratory syndrome coronavirus (MERS-CoV), both transmitted from animals to humans, triggered global epidemics, in 2003 and 2012, respectively, with high mortality rates.[1] In December 2019, a coronavirus infectious disease (named COVID-19) was detected in Wuhan, province of Hubei, China, caused by a new pathogenic CoV, named SARS-CoV-2. The virus spread very rapidly from China to all countries, and on March 11th, 2020, it was declared a pandemic by the World Health Organization (WHO). At the time of this writing, there are over 20 million cases worldwide, with more than 750.000 fatalities;[2] no country has been spared of this disease. The mortality rate of the SARS-CoV-2 is currently estimated in the range of 0.5–6%; and while COVID-19 appears to be less deadly than SARS (~10%)[3] or MERS (~40%),[3] it seems to be more contagious, with a reproductive number (R_o) in the range 2.0–6.5,[4] higher than SARS and MERS, which could explain the velocity of its propagation.

Today, no specific therapeutics is available, and current disease management is limited to social measures, such as social distancing, travel ban, and full lockdown in many cities. Thus, there is an urgent need for the discovery of prevention and treatment strategies for the COVID-19. It is acknowledged that the development and evaluation of a vaccine might take at least a year; moreover, vaccine development should be observant of all safety and regulatory issues.[5] While the discovery and evaluation of a new drug should take even longer, the use of an existing drug (or compound undergoing clinical trials) to treat COVID-19 (drug repurposing) seems the fastest strategy, since these compounds have either regulatory approval as drugs or have cleared safety studies that indicate a therapeutic potential.[6]

Very recently, 332 SARS-CoV-2-human protein-protein interactions were identified, and 69 compounds – including several FDA-approved drugs, were found to be effective against 66 of those human proteins or host factors.[7] At the same time, experimental structures of several SARS-CoV-2

[a] C. N. Cavasotto, J. I. Di Filippo
Computational Drug Design and Biomedical Informatics Laboratory, Translational Medicine Research Institute (IIMT), CONICET-Universidad Austral
Pilar, Buenos Aires, Argentina
E-mail: CCavasotto@austral.edu.ar
cnc@cavasotto-lab.net

[b] C. N. Cavasotto
Facultad de Ciencias Biomédicas and Facultad de Ingeniería, Universidad Austral
Pilar, Buenos Aires, Argentina

[c] C. N. Cavasotto
Austral Institute for Applied Artificial Intelligence
Pilar, Buenos Aires, Argentina

Supporting information for this article is available on the WWW under https://doi.org/10.1002/minf.202000115

proteins have become increasingly available, such as the main protease (M^{pro}), and the papain-like protease (PL^{pro}) (non-structural protein 5 (nsp5) and nsp3, respectively), the RNA-dependent RNA-polymerase (nsp12-nsp7-nsp8), the dimer nsp14-nsp10 (which harbours the exoribonuclease and the guanine-N7 methyl transferase functions), the dimer nsp16-nsp10, which functions as a 2′-O-methyl transferase, among others. The identification of host targets coupled with the availability of viral proteins enhances the possibility of identifying COVID-19 therapeutic strategies through drug repurposing.

While some pharmaceuticals are currently being tested,[8] there is a clear need to develop new alternatives within the drug repurposing approach. In this contribution, we perform molecular docking-based virtual screening using a chemical library built from approved Food and Drug Administration (FDA) drugs and compounds undergoing clinical trial on the following three viral target proteins: the spike glycoprotein (S-protein), and two proteases, namely, the 3-chymotrypsin-like protease $3CL^{pro}$ (or M^{pro}) and the PL^{pro}. The S-protein binds directly to the Angiotensin Converting Enzyme 2 (ACE2) receptor of the human host cell surface -thus enabling virus entry and replication, and the two proteases process the two viral polyproteins encoded by the open reading frames (ORFs) orf1a and orf1b. It has been shown that the PL^{pro} also have de-ubiquitination and de-ISGylation activities in SARS and MERS.

Using a quantum mechanical (QM) scoring,[9] and consensus ranking,[10] from our virtual screening, we suggest a variety of compounds (either FDA-approved or in clinical trials) that may inhibit SARS-CoV-2. Needless to say, these compounds should be evaluated in *ad hoc* experimental assays and clinical trials to confirm their actual activity against COVID-19. This contribution complements earlier works in the field,[11] and it is our hope to thus collaborate to the worldwide efforts to deliver a prompt answer to the deadly threat of COVID-19.

2 Materials and Methods

2.1 Molecular System Setup

The following structures were downloaded from the Protein Data Bank (PDB) and prepared using the ICM software[12] (MolSoft, San Diego, CA, 2019): the SARS-CoV-2 M^{pro} covalently bound to the peptide-like inhibitor N3 (PDB 6LU7, resolution 2.16 Å), and its unbound form (PDB 6YB7, 1.25 Å); the SARS-CoV PL^{pro} complexed with non-covalent ligand GRL0617 (PDB 3E9S, 2.5 Å); the SARS-CoV-2 PL^{pro} with covalent ligand VIR251 (Ac-hTyr-Dap-Gly-Gly-VME) (PDB 6WX4, 1.65 Å); the SARS-CoV-2 S-protein bound to ACE2 (PDB 6 M17, 2.9 Å). Regarding the molecular system preparation, hydrogen atoms were added, followed by a short local energy minimization in the torsional space; the positions of polar and water hydrogens were determined by optimizing the hydrogen bonding network, and then all water molecules were deleted. All Asp and Glu residues were assigned a -1 charge, and all Arg and Lys residues were assigned a $+1$ charge. Asn and Gln residues were inspected, and their amide group eventually flipped according to the neighboring hydrogen bond network. Histidine tautomers were selected in a similar way. Covalently bound ligands N3 (M^{pro}), and VIR251 (PL^{pro}) were detached from their corresponding structures, the corresponding linking cysteines (C145 for M^{pro}, and C111 for PL^{pro}) were restored to their normal S-protonated structure, and a hydrogen was added to N3 and VIR251 at their attachment carbons.

To account for conformational diversity, we also built a model of SARS-CoV-2 PL^{pro} using the structure of SARS-CoV PL^{pro} non-covalently bound to the benzamide derivative GRL0617 (PDB 3E9S) as template; this structure performed slightly better in redocking experiments compared to other SARS-CoV PL^{pro} structures of similar resolution (PDBs 4OW0, 4MM3 (apo), and 4OVZ). The two proteins are highly similar (82% sequence identity), with full amino acid conservation within the binding site (Figure S1, Supporting Information). A crude model was built using the backbone structure of the template, and then refined through local energy minimization using ICM. To avoid pocket collapse, and taking into account the complete conservation of the binding site, ligand GRL0617 was kept during the refinement process, in a ligand-steered modelling fashion.[13]

2.2 Database Preparation

The docking library was constructed by merging molecule subsets from four different libraries: i) ChEMBL (Version 26)[14] (including molecules which reached at least Phases 1, 2, 3 or 4); ii) DrugBank Version 5.1.5.[15] (including chemical databases of Approved, Experimental and Investigational drugs); iii) the DrugCentral database of approved drugs;[16] iv) the FDA-approved library from Selleck Chemicals (www.selleckchem.com). Redundant entries were eliminated, and metals and molecules with less than six, or more than 120 atoms were deleted, totalizing 11552 molecules. Compounds N3 (ligand of 6LU7) and VIR251 (ligand of 6WX4) were added to the library for redocking purposes.

2.3 High-throughput Docking

For M^{pro} and PL^{pro}, the catalytic binding sites were considered, while the docking boxes were built large enough to have at least 5 Å from their boundaries to any atom of the associated ligands (N3 for M^{pro}, VIR251 and GRL0617 for PL^{pro}); for the S-protein, the docking box boundaries were at least 5 Å from every atom of the interface of S-protein with ACE2. Molecular docking was

performed with ICM using a rigid-receptor:flexible-molecule docking approach. The receptor was represented by six potential energy maps, while the docked molecule was considered flexible, with its six positional degrees of freedom (three translational and three rotational), and its internal dihedral angles considered free. Starting from a randomized conformation, each molecule was subjected to a global energy minimization protocol within the potential of the receptor, that consists of a Monte-Carlo sampling with local energy minimization of the differentiable variables after each random step.[12] The lowest energy pose for each molecule was assigned an ICM empirical score according to its fit within the binding site.[17]

2.4 Quantum Mechanical Scoring

Protein-molecule complexes generated using the rigid-receptor:flexible-molecule docking module in ICM were further optimized through cycles of local energy minimization in the torsional space using ICM, where all amino-acids within 4 Å of any docked molecule were considered free. After performing this structural relaxation, for each target all amino-acids within 8 Å of any docked molecule were then listed, and used to build a reduced system, capping the N- and C-terminal of each fragment of the cut-out system with hydrogens (cf. Ref.[9c] for details on the relaxation process and system cutout).

The quantum mechanical docking score[9c] (*QMDS*) on the reduced system was calculated according to

$$QMDS = \Delta G_o^{QM} + \Delta G_{conf}^{QM}(P) + \Delta G_{conf}^{QM}(L) - T\Delta S \quad (1)$$

where the "o" subscript in the first term refers to the difference of the free energy calculated using the protein-ligand (PL), protein (P) and ligand (L) conformations from the docked complex, the fourth term corresponds to the change in conformational entropy, and the second and third terms are calculated as

$$\Delta G_{Conf}^{QM} = G_o^{QM}(X) + G^{QM}(X), (X = L, P) \quad (2)$$

where $G_o^{QM}(X)$ is the energy of the isolated X in the conformation of the docked PL complex, and $G^{QM}(X)$ is the energy of X in the free unbound state. The unbound states were generated through local energy minimization on both protein and molecule in isolation.

The binding conformational entropy was calculated as

$$\Delta S = R \ln \frac{\Omega_{bound}}{\Omega_{free}} \quad (3)$$

where Ω is the number of structural conformations. It was assumed that upon binding the molecule adopts a single conformational state (thus $\Omega_{bound} = 1$), and Ω_{free} (the number of diverse torsional conformations of the molecule in its free state) was calculated by performing a Monte-Carlo (MC) sampling with local energy minimization in the torsional space using ICM,[12,18] and collecting all structurally different conformations within the lowest 3 kcal/mol energy (it was further assumed that all conformers were equally probable).

QM calculations were performed using the MOPAC2016 software[19] and its linear-scaling module MOZYME,[20] using the semi-empirical PM7 Hamiltonian.[21] The PM7 Hamiltonian includes several corrections to the PM6 Hamiltonian,[22] accounts for dispersion interactions, while hydrogen and halogen bonding effects have been taken into consideration at the parameterization stage.[23] PM7 also exhibited a very good performance at discriminating native ligand positions in crystallographic complexes.[24] The solvation energy contribution in aqueous environment was calculated according to the Conductor Like Screening Model (COSMO),[25] continuum solvent model, with default atomic radii and surface tension parameters. The solvent-accessible surface area was extracted from the MOPAC2016 output (cf. http://openMOPAC.net for details).

2.5 Consensus Scoring

The rankings built using docking scores from ICM and QMDS were combined according to the Exponential Consensus Ranking (ECR),[10] were a consensus rank *ECR*(*i*) for each molecule *i* was calculated using a sum of exponential distributions as a function of the molecule rank built from individual scoring functions *j*, according to

$$ECR(i) = \frac{1}{\sigma} \sum_j \exp\left[-\frac{r_j(i)}{\sigma} \right] \quad (4)$$

where $r_j(i)$ is the rank of molecule *i* using the scoring function *j*, and σ is the expected value of the exponential distribution; the *ECR* was found to be basically independent on σ,[10] and we used $\sigma = 10$. It should be noted that the ECR was evaluated on several benchmark systems using individual and multiple target structures from diverse protein families, and it was found that it outperformed traditional consensus strategies over a wide range of systems.[10] Since it is based on rank rather than score, it is independent of score units, scales and offsets.

2.6 Flexible Molecular Docking to Multiple Receptor Conformations

To account for target flexibility upon docking, a multiple receptor conformations docking approach[26] was used for M^{pro} and PL^{pro}. For each target, docking is performed independently onto several structures (in this case, two), and for each structure, molecule rankings calculated using ICM and QMDS scoring are combined into the ECR. The hit-lists corresponding to each target structure are then merged, and the best ECR for each molecule was kept according to the merging-and-shrinking method.[27]

3 Results and Discussion

We docked a chemical library of 11.552 compounds (composed by FDA-approved, investigational and experimental drugs, cf. the Materials and Methods section for details) onto three different target proteins of the SARS-CoV-2: the M^{pro}, the PL^{pro}, and the S-protein. In all targets, molecules were scored with ICM and with the recently developed QM docking score (QMDS),[9c] in the latter case accounting also for receptor and small-molecule deformation. It should be highlighted that QM methods capture the underlying physics of the molecular system accounting for all energy contributions, including electronic polarization, covalent-bond formation, and charge transfer.[9b,28] For each individual structure, the exponential consensus ranking (ECR, see Methods) was calculated combining the individual rankings built using ICM and QMDS scoring. For M^{pro} and PL^{pro} the multiple receptor conformations approach was used, and ECR rankings were combined using the merging-and-shrinking procedure (cf. Materials and Methods). In all three targets, the 2% top-ranking molecule subset was then analyzed, selecting candidates in terms of their ECR, the presence of key interactions with the receptor, physicochemical properties, and visual inspection.

For the M^{pro}, two experimental structures were used in docking: M^{pro} bound to peptide-like N3 (PDB 6LU7)[29] and the unbound form of the protein (PDB 6YB7). The purpose of using two structures for docking is to account, at least to some extent, for protein flexibility by using the multiple receptor conformations approach;[26] Self-docking of the co-crystallized peptide-like N3 onto structure 6LU7 had a root-medium-square deviation (RMSD) of 1.6 Å, an excellent result for a flexible peptide, originally covalently bound to the structure; according to its ECR, N3 was within the top 0.4% of the docked library, what constitutes a simple but necessary validation of the docking approach.

According to the docking protocol described above, the following drugs can be listed as potential inhibitors of the SARS-CoV-2 M^{pro}: Sovaprevir (ChEMBL ID CHEMBL2105750), an experimental drug designed to treat the hepatitis C virus (HCV) and that acts as a NS3/4 A inhibitor (it should be mentioned that another NS3/4 A inhibitor, Danoprevir, is in clinical trials against COVID-19;[30] Samatasvir (CHEMBL3039519), an investigational drug that has been used in trials as a treatment for hepatitis C infection, and acts as a NS5 A inhibitor; Candesartan Cilexetil (CHEMBL1014), a type-1 angiotensin II receptor (AT_1) blocker used mainly for the treatment of high blood pressure and congestive heart failure; Saquinavir (CHEMBL114), Ritonavir (DrugBank ID DB00503) (cf. Figure 1), and Indinavir

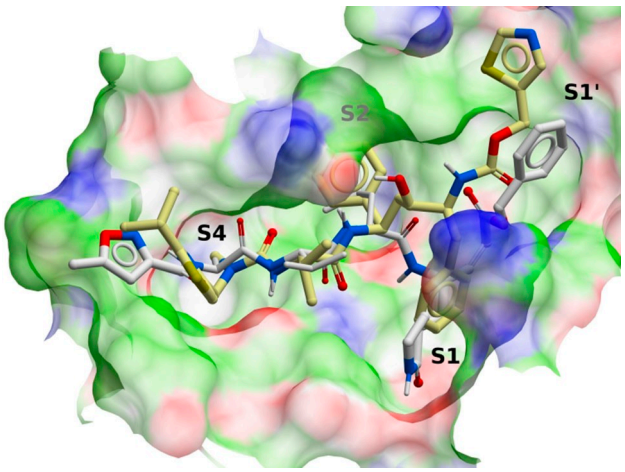

Figure 1. Ritonavir docked within the binding site of SARS-CoV-2 M^{pro}. The binding site surface is colored as: red, oxygens; blue, nitrogen; white, polar hydrogen; green, non-polar atoms. The co-crystallized peptide-like ligand N3 (6LU7) is also displayed with white carbon atoms superimposed to Ritonavir (yellow carbons). The binding site sub-sites S1, S1′, S2 and S4 are also shown. Figure prepared with ICM (Molsoft LLC, San Diego, CA).

(DB00224), which are FDA-approved drugs which act as HIV protease inhibitors and are used to treat HIV/AIDS; Brilacidin (CHEMBL2219413), an investigational drug for the supportive care of mucositis, stomatitis, and head and neck neoplasms (interestingly, Brilacidin is being investigated for direct inhibition of SARS-CoV-2 (press release of April 6th, 2020 (www.ipharminc.com/press-release); Flovagatran (DB05714), an investigational drug that acts as a thrombin inhibitor; Aplidin (plitidepsin, CHEMBL2447908), a Phase II drug for myeloma, and currently undergoing clinical trials for COVID-19 (myelomaresearchnews.com/2020/04/20/); Tomivosertib (DB15219) is an investigational drug in clinical trials for triple negative breast cancer and hepatocellular carcinoma; Rebamipide (DB11656) is an investigational drug for the treatment of stomach ulcer, gastric adenoma and early gastric cancer; Eribaxaban (DB06920) is an experimental drug which inhibits the coagulation factor X; DB07451 is an experimental drug being investigated for targeting the Gal-Pol protein; ENMD-981693 (DB05608) is an investigational drug for the treatment in breast cancer, leukemia, lung cancer, and solid tumors. Other investigational drugs include DB02747, DB04692, and DB03311, whose applica-

tion and/or use have not been yet disclosed. Considering the large size of the binding site, other larger molecules have been identified, such as Felypressin (DB00093), an investigational synthetic peptide used as a vasoconstrictor. The list of potential inhibitors of the M^{pro} is summarized in Table 1, and the structures of these compounds are shown in Figure S2 (Supporting Information).

Table 1. Potential inhibitors of SARS-CoV-2 M^{pro} from existing drugs and compounds undergoing clinical trials.

Compound name	Compound ID
ENMD-981693	DB05608
Felypressin	DB00093
Brilacidin	CHEMBL2219413
	DB03311[a]
Samatasvir	CHEMBL3039519
Eribaxaban	DB06920
Aplidin	CHEMBL2447908
Candesartan Cilexetil	CHEMBL1014
Ritonavir	CHEMBL163
Tomivosertib	DB15219
Rebamipide	DB11656
Saquinavir	CHEMBL114
	DB02747[b]
	DB07451[c]
Flovagatran	DB05714
Sovaprevir	CHEMBL2105750
	DB04692[d]
Indinavir	DB00224

[a]3-(3,5-dibromo-4-hydroxy-benzoyl)-2-ethyl-benzofuran-6-sulfonic Acid [4-(thiazol-2-ylsulfamoyl)-phenyl]-amide. [b]Diamino-n-[(4s)-5-anilino-4-{[(2s)-2-{[(1r)-1-carboxyethyl]amino}-4-phenylbutanoyl]amino}-5-oxopentyl]methaniminium. [c]1-(5-bromo-pyridin-2-yl)-3-[2-(6-fluoro-2-hydroxy-3-propionyl-phenyl)-cyclopropyl]-urea. [d]Ethyl (2e)-4-({(2s)-2-[(n-{[(2-methyl-2-propanyl)oxy]carbonyl}-l-valyl)amino]-2-phenylacetyl}amino)-5-[(3s)-2-oxo-3-pyrrolidinyl]-2-pentenoate

It should be highlighted that targeting PL^{pro} with antiviral drugs may not only block viral replication, but could also inhibit the dysregulation of signaling cascades in infected cells that may lead to cell death in other uninfected cells.[31] Very recently, two SARS-CoV-2 PL^{pro} crystal structures were made available with peptide-like ligands VIR250 and VIR251 covalently attached to C111, at 2.8 Å (PDB 6WUU) and 1.7 Å resolution (PDB 6WX4), respectively.[32] These structures are very similar to the unbound PL^{pro} crystal structures 6W9C, 6WZU, and 6WRH (at 2.7 Å, 1.8 Å, 1.6 Å resolution, respectively), exhibiting with respect to them an overall backbone RMSD of 0.9 Å, and 0.4 Å for amino acids within the VIR250 and VIR251 binding sites.

The SARS-CoV PL^{pro} complexed with the benzamide inhibitor GRL0617[33] (PDB 3E9S) is structurally very similar to the SARS-CoV-2 PL^{pro} structures mentioned above, what is not surprising since both proteases share a high 82% sequence identity, and 100% within the binding site; however, the SARS-CoV structure displays a slightly different conformation of the β-hairpin (N267-C270) close to the binding site. In order to incorporate target conformational diversity in the docking protocol, and considering that benzamides have been reported to bind to SARS-CoV and MERS-CoV PL^{pro},[34] we built a homology model of SARS-CoV-2 PL^{pro} using the PDB 3E9S template. Our model exhibited very low backbone RMSD (less than 1 Å) compared to all SARS-CoV-2 PL^{pro} structures (6W9C, 6WZU, 6WRH, 6WUU, and 6WX4), while conserving the differentiating β-hairpin structural feature of SARS-CoV PL^{pro}.

For docking-based virtual screening we used the bound SARS-CoV-2 PL^{pro} structure with the lowest resolution available (PDB 6WX4), and the model built using template 3E9S. As it has been said, using two structures is a way to partially account for protein flexibility in docking.[26] Re-docking of VIR251 onto 6WX4, and GRL0617 onto the model yielded RMSD values of 1.0 Å and 0.4 Å, respectively; according to their ECR, both ligands were within the top 0.2% and the top 0.4% of the screened database, respectively, what could be considered as a validation of our approach.

From our analysis based on the criteria mentioned above, we identified several potential inhibitors of PL^{pro}, of which we can highlight the following: Pilaralisib (CHEMBL3360203), an orally available selective small-molecule that inhibits the phosphoinositide-3 kinase (PI3 K), that has been used in trials studying the treatment of different types of cancer, such as lymphoma, solid tumors, and glioblastoma; Tiracizine (DB13635) (cf. Figure 2), a dibenzazepine and an experimental anti-arrhythmic agent; Compound DB07665, an experimental drug which targets prothrombin; Cilazapril (DB01340), an FDA-approved ACE inhibitor for the treatment of hypertension and heart failure (cilazapril is in fact a progrud that is hydrolyzed to its main metabolite cilaprilat, although the structural differences of the prodrug and its active form share the same pose within the binding site); Indisulam (CHEMBL77517), a sulfonamide investigational compound with potential antineoplastic activity, which inhibits the cyclin-dependent kinase (CDK), which is usually over-expressed in cancerous cells; compound DB03082, an experimental naphtamide derivative which shows activity as a urokinase-type plasminogen activator; Picotamide (DB13327), an experimental antiplatelet agent which acts as a thromboxamne synthase inhibitor and a thromboxane receptor inhibitor; the benzamide derivative DB08656 corresponds to GRL6017, which is a potent, selective and competitive noncovalent inhibitor of SARS-CoV PL^{pro}, exhibiting an IC_{50} of 0.6 μM, and a K_i of 0.49 μM;[33] Anatibant (CHEMBL2107725), a selective, potent, small-molecule antagonist of the Bradykinin B2 receptor, developed for the treatment of traumatic brain injury; BMSC-0013 (DB02474) (cf. Figure 2), an investigational drug targeting the cholera enterotoxin subunit B; Zabofloxacin (CHEMBL2107811), an investigational drug that has been

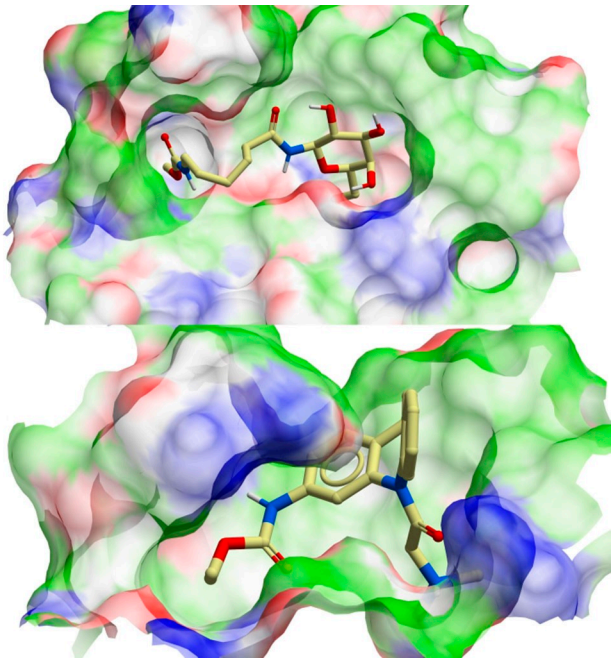

Figure 2. Compound BMSC-0013 (upper panel) and Tiracizine (lower panel) docked within the binding site of SARS-CoV-2 PL^{pro}. The binding site surface is colored as: red, oxygens; blue, nitrogen; white, polar hydrogen; green, non-polar atoms. Figure prepared with ICM (Molsoft LLC, San Diego, CA).

used in trials for the treatment of community acquired pneumonia; compound DB07533, a thiazolidinone inhibitor of CDK2; Ziprasidone (DB00246), an FDA-approved drug to treat schizophrenia and bipolar disorder; Darolutamide (DB12941), an FDA-approved nonsteroidal androgen receptor antagonist for the treatment of castrate-resistant, non-metastatic prostate cancer; Propamidine (CHEMBL23013), whose application has not been yet released. The list of potential inhibitors of the PL^{pro} is summarized in Table 2, and the structures of these compounds are listed in Figure S3 (Supporting Information).

The SARS-CoV-2 spike-protein (S-protein) receptor binding domain (RBD) binds to the ACE2 receptor in the host cell, and thus may represent an attractive drug target. Experimental structures of the RBD in complex with ACE2 have been very recently obtained,[35] so we isolated the RBD from one of them (PDB 6LZG), and docked and scored our library of approved drugs. It should be borne in mind that the RBD interface that should be targeted to preclude its interaction with ACE2 is not a buried binding site, a somehow shallow surface. Thus, the top scoring compounds are usually large and flexible molecules, and further validation using, for example, molecular dynamics, should be considered for prioritizing compounds before any sort of experimental evaluation. Potential inhibitors include Pralatrexate (DB06813), which is an approved drug for the treatment of relapsed or refractory peripheral T-cell lymphoma; Carumonam (DB13553), an experimental antimicrobial drug, Bradykinin (DB12126), which has been investigated for the treatment of hypertension and type 2 diabetes; Aclerastide (DB12631), an investigational drug for the treatment of diabetic foot; granotapide (CHEMBL 4297618), which has been used in trials for the treatment of type 2 diabetes mellitus; DB05616, a phase II investigational drug being investigated as an antirheumatic agent. The list of potential inhibitors of the S-protein is summarized in Table 3.

Table 2. Potential inhibitors of SARS-CoV-2 PL^{pro} from existing drugs and compounds undergoing clinical trials.

Compound name	Compound ID
Anatibant	CHEMBL2107725
	DB03082[a]
Pilaralisib	CHEMBL3360203
Tiracizine	DB13635
BMSC-0013	DB02474
	DB07533[b]
Zabofloxacin	CHEMBL2107811
	DB07665[c]
Picotamide	DB13327
Cilazapril	DB01340
Indisulam	CHEMBL77517
	DB08656[d]
Darolutamide	DB12941
Ziprasidone	DB00246
Propamidine	CHEMBL23013

[a]6-[(z)-amino(imino)methyl]-n-[4-(aminomethyl)phenyl]-4-(pyrimidin-2-ylamino)-2-naphthamide. [b]4-{5-[(z)-(2-imino-4-oxo-1,3-thiazolidin-5-ylidene)methyl]-2-furyl}-n-methylbenzenesulfonamide. [c]N-[2-(carbamimidamidooxy)ethyl]-2-{6-cyano-3-[(2,2-difluoro-2-pyridin-2-ylethyl)amino]-2-fluorophenyl}acetamide. [d]5-amino-2-methyl-n-[(1r)-1-naphthalen-1-ylethyl]benzamide

Table 3. Potential inhibitors of SARS-CoV-2 S-protein from existing drugs and compounds undergoing clinical trials.

Compound name	Compound ID
Pralatrexate	DB06813
Carumonam	DB13553
Aclerasteride	DB12634
Granotapide	CHEMBL4297618
	DB05616[a]

[a]4′-Methylene-5,8,10-trideazaaminopterin

4 Conclusions

The infectous respiratory disease COVID-19 originated in Wuhan, China in December 2019, and rapidly expanding throughout the world is a most serious threat to global health, totalizing at the time of this writing over 20 million infected people, and more than 750,000 fatalities. So far, neither a vaccine nor an approved drug are currently

available to treat this disease. Considering the time required to develop any of these options, drug repurposing seems the most appealing and straightforward approach. In this contribution, we performed docking-based virtual screening on three SARS-CoV-2 targets (the proteases M^{pro} and PL^{pro}, and the spike glycoprotein) using an in-house library of FDA-approved, investigational and experimental drugs to suggest potential compounds which may act as antivirals. A novel QM scoring methodology coupled with consensus scoring, and accounting for target flexibility was used. While further experimental validation and clinical trials are necessary to confirm their activity against COVID-19, we join our effort to that of many other researchers to come up with an urgent and effective solution to this threat.

Conflict of Interest

None declared.

Acknowledgements

The Authors thank Dr. Julián Maggini, Dr. Mariano Núñez, and Dr. Ventura Simonovich for helful discussions. This work was supported by the National Agency for the Promotion of Science and Technology (ANPCyT) (PICT-2014-3599 and PICT-2017-3767). CNC thanks Molsoft LLC (San Diego, CA) for providing an academic license for the ICM program. The authors are grateful to the National System of High Performance Computing (Sistemas Nacionales de Computación de Alto Rendimiento, SNCAD), and the Centro de Cálculo de Alto Desempeño (Universidad Nacional de Córdoba) for granting use of their computational resources.

References

[1] C. I. Paules, H. D. Marston, A. S. Fauci, *JAMA* **2020**, *323*, 707–708.
[2] World Health Organization, **2020**, pp. Coronavirus disease (COVID-19) – Situation Report – 156.
[3] W. S. Lim, in *ERS Handbook of Respiratory Medicine* (Eds.: P. Palange, G. Rohde), European Respiratory Society, **2019**, pp. 393–399.
[4] Y. Liu, A. A. Gayle, A. Wilder-Smith, J. Rocklöv, *J. Travel Med.* **2020**, *27*.
[5] S. Jiang, *Nature* **2020**, *579*, 321.
[6] R. K. Guy, R. S. DiPaola, F. Romanelli, R. E. Dutch, *Science* **2020**, *368*, 829–830.
[7] D. E. Gordon, G. M. Jang, M. Bouhaddou, J. Xu, K. Obernier, K. M. White, M. J. O'Meara, V. V. Rezelj, J. Z. Guo, D. L. Swaney, T. A. Tummino, R. Huettenhain, R. M. Kaake, A. L. Richards, B. Tutuncuoglu, H. Foussard, J. Batra, K. Haas, M. Modak, M. Kim, P. Haas, B. J. Polacco, H. Braberg, J. M. Fabius, M. Eckhardt, M. Soucheray, M. J. Bennett, M. Cakir, M. J. McGregor, Q. Li, B. Meyer, F. Roesch, T. Vallet, A. Mac Kain, L. Miorin, E. Moreno, Z. Z. C. Naing, Y. Zhou, S. Peng, Y. Shi, Z. Zhang, W. Shen, I. T. Kirby, J. E. Melnyk, J. S. Chorba, K. Lou, S. A. Dai, I. Barrio-Hernandez, D. Memon, C. Hernandez-Armenta, J. Lyu, C. J. P. Mathy, T. Perica, K. B. Pilla, S. J. Ganesan, D. J. Saltzberg, R. Rakesh, X. Liu, S. B. Rosenthal, L. Calviello, S. Venkataramanan, J. Liboy-Lugo, Y. Lin, X. P. Huang, Y. Liu, S. A. Wankowicz, M. Bohn, M. Safari, F. S. Ugur, C. Koh, N. S. Savar, Q. D. Tran, D. Shengjuler, S. J. Fletcher, M. C. O'Neal, Y. Cai, J. C. J. Chang, D. J. Broadhurst, S. Klippsten, P. P. Sharp, N. A. Wenzell, D. Kuzuoglu, H. Y. Wang, R. Trenker, J. M. Young, D. A. Cavero, J. Hiatt, T. L. Roth, U. Rathore, A. Subramanian, J. Noack, M. Hubert, R. M. Stroud, A. D. Frankel, O. S. Rosenberg, K. A. Verba, D. A. Agard, M. Ott, M. Emerman, N. Jura, et al., *Nature* **2020**, *583*, 459–468.
[8] a) G. Li, E. De Clercq, *Nat. Rev. Drug Discovery* **2020**, *19*, 149–150; b) M. Wang, R. Cao, L. Zhang, X. Yang, J. Liu, M. Xu, Z. Shi, Z. Hu, W. Zhong, G. Xiao, *Cell Res.* **2020**, *30*, 269–271; c) H. Ledford, *Nature* **2020**, *581*, 247–248.
[9] a) M. G. Aucar, C. N. Cavasotto, *Methods Mol. Biol.* **2020**, *2114*, 269–284; b) C. N. Cavasotto, N. S. Adler, M. G. Aucar, *Front. Chem.* **2018**, *6*, 188; c) C. N. Cavasotto, M. G. Aucar, *Front. Chem.* **2020**, *8*, 246.
[10] K. Palacio-Rodriguez, I. Lans, C. N. Cavasotto, P. Cossio, *Sci. Rep.* **2019**, *9*, 5142.
[11] a) S. Khaerunnisa, H. Kurniawan, R. Awaluddin, S. Suhartati, S. Soetjipto, *Preprints* **2020**, doi: 10.20944/preprints202003.200226.v202001; b) Z. Xu, C. Peng, Y. Shi, Z. Zhu, K. Mu, X. Wang, W. Zhu, *bioRxiv* **2020**, 10.1101/2020.1101.1127.921627; c) M. Smith, J. C. Smith, *ChemRxiv* **2020**, https://doi.org/10.26434/chemrxiv.11871402.v11871404; d) Y. Zhou, Y. Hou, J. Shen, Y. Huang, W. Martin, F. Cheng, *Cell Discovery* **2020**, *6*, 14; e) A. Contini, *ChemRxiv* **2020**, https://doi.org/10.26434/chemrxiv.11847381.v11847381; f) A. Fischer, M. Sellner, S. Neranjan, M. A. Lill, M. Smieško, *ChemRxiv* **2020**, https://doi.org/10.26434/chemrxiv.11923239.v11923232; g) A.-T. Ton, F. Gentile, M. Hsing, F. Ban, A. Cherkasov, *Mol. Inf.* **2020**, doi:10.1002/minf.202000028; h) J. Wang, *ChemRxiv* **2020**, https://doi.org/10.26434/chemrxiv.11875446.v11875441.
[12] R. Abagyan, M. Totrov, D. Kuznetsov, *J. Comput. Chem.* **1994**, *15*, 488–506.
[13] a) C. N. Cavasotto, A. J. Orry, N. J. Murgolo, M. F. Czarniecki, S. A. Kocsi, B. E. Hawes, K. A. O'Neill, H. Hine, M. S. Burton, J. H. Voigt, R. A. Abagyan, M. L. Bayne, F. J. Monsma, Jr., *J. Med. Chem.* **2008**, *51*, 581–588; b) C. N. Cavasotto, D. Palomba, *Chem. Commun.* **2015**, *51*, 13576–13594; c) S. S. Phatak, E. A. Gatica, C. N. Cavasotto, *J. Chem. Inf. Model.* **2010**, *50*, 2119–2128.
[14] A. Gaulton, A. Hersey, M. Nowotka, A. P. Bento, J. Chambers, D. Mendez, P. Mutowo, F. Atkinson, L. J. Bellis, E. Cibrián-Uhalte, M. Davies, N. Dedman, A. Karlsson, M. P. Magariños, J. P. Overington, G. Papadatos, I. Smit, A. R. Leach, *Nucleic Acids Res.* **2017**, *45*, D945-D954.
[15] D. S. Wishart, Y. D. Feunang, A. C. Guo, E. J. Lo, A. Marcu, J. R. Grant, T. Sajed, D. Johnson, C. Li, Z. Sayeeda, N. Assempour, I. Iynkkaran, Y. Liu, A. Maciejewski, N. Gale, A. Wilson, L. Chin, R. Cummings, D. Le, A. Pon, C. Knox, M. Wilson, *Nucleic Acids Res.* **2018**, *46*, D1074-D1082.
[16] O. Ursu, J. Holmes, J. Knockel, C. G. Bologa, J. J. Yang, S. L. Mathias, S. J. Nelson, T. I. Oprea, *Nucleic Acids Res.* **2017**, *45*, D932-D939.
[17] M. Totrov, R. Abagyan, in *RECOMB '99: Proceedings of the Third Annual International Conference on Computational Molecular Biology* (Eds.: S. Istrail, P. Pevzner, M. Waterman), Associaton for

Computer Machinery, New York, Lyon, France, **1999**, pp. 37–38.
[18] R. Abagyan, M. Totrov, *J. Mol. Biol.* **1994**, *235*, 983–1002.
[19] J. J. P. Stewart, *MOPAC2016*, Stewart Computational Chemistry, http://OpenMOPAC.net, Colorado Springs, CO, **2016**.
[20] J. J. P. Stewart, *Int. J. Quantum Chem.* **1996**, *58*, 133–146.
[21] J. J. Stewart, *J. Mol. Model.* **2013**, *19*, 1–32.
[22] J. J. P. Stewart, *J. Mol. Model.* **2007**, *13*, 1173–1213.
[23] A. V. Sulimov, D. C. Kutov, E. V. Katkova, I. S. Ilin, V. B. Sulimov, *J. Mol. Graphics Modell.* **2017**, *78*, 139–147.
[24] A. V. Sulimov, D. C. Kutov, E. V. Katkova, V. B. Sulimov, *Advances in bioinformatics* **2017**, *2017*, 7167691.
[25] A. Klamt, G. Schüürmann, *J. Chem. Soc. Perkin Trans.* **1993**, *2*, 799–805.
[26] a) C. N. Cavasotto, N. Singh, *Curr. Comput.-Aided Drug Des.* **2008**, *4*, 221–234; b) F. Spyrakis, C. N. Cavasotto, *Arch. Biochem. Biophys.* **2015**, *583*, 105–119; c) M. Totrov, R. Abagyan, *Curr. Opin. Struct. Biol.* **2008**, *18*, 178–184.
[27] a) C. N. Cavasotto, R. A. Abagyan, *J. Mol. Biol.* **2004**, *337*, 209–225; b) C. N. Cavasotto, J. A. Kovacs, R. A. Abagyan, *J. Am. Chem. Soc.* **2005**, *127*, 9632–9640.
[28] C. N. Cavasotto, M. G. Aucar, N. S. Adler, *Int. J. Quantum Chem.* **2019**, *119*, e25678.
[29] Z. Jin, X. Du, Y. Xu, Y. Deng, M. Liu, Y. Zhao, B. Zhang, X. Li, L. Zhang, C. Peng, Y. Duan, J. Yu, L. Wang, K. Yang, F. Liu, R. Jiang, X. Yang, T. You, X. Liu, X. Yang, F. Bai, H. Liu, X. Liu, L. W. Guddat, W. Xu, G. Xiao, C. Qin, Z. Shi, H. Jiang, Z. Rao, H. Yang, *Nature* **2020**, *582*, 289–293.
[30] H. Chen, Z. Zhang, L. Wang, Z. Huang, F. Gong, X. Li, Y. Chen, J. J. Wu, *medRxiv* **2020**, 2020.2003.2022.20034041.
[31] Y. M. Baez-Santos, S. E. St. John, A. D. Mesecar, *Antiviral Res.* **2015**, *115*, 21–38.
[32] W. Rut, Z. Lv, M. Zmudzinski, S. Patchett, D. Nayak, S. J. Snipas, F. El Oualid, T. T. Huang, M. Bekes, M. Drag, S. K. Olsen, *bioRxiv* **2020**, 2020.2004.2029.068890.
[33] K. Ratia, S. Pegan, J. Takayama, K. Sleeman, M. Coughlin, S. Baliji, R. Chaudhuri, W. Fu, B. S. Prabhakar, M. E. Johnson, S. C. Baker, A. K. Ghosh, A. D. Mesecar, *Proc. Natl. Acad. Sci. USA* **2008**, *105*, 16119–16124.
[34] H. Lee, H. Lei, B. D. Santarsiero, J. L. Gatuz, S. Cao, A. J. Rice, K. Patel, M. Z. Szypulinski, I. Ojeda, A. K. Ghosh, M. E. Johnson, *ACS Chem. Biol.* **2015**, *10*, 1456–1465.
[35] a) R. Yan, Y. Zhang, Y. Li, L. Xia, Y. Guo, Q. Zhou, *Science* **2020**, *367*, 1444–1448; b) Q. Wang, Y. Zhang, L. Wu, S. Niu, C. Song, Z. Zhang, G. Lu, C. Qiao, Y. Hu, K. Y. Yuen, H. Zhou, J. Yan, J. Qi, *Cell* **2020**, *181*, 894–904 e899.

Received: May 12, 2020
Accepted: July 28, 2020
Published online on August 18, 2020

